Progress In Electromagnetics Research Letters, Vol. 89, 29–36, 2020

An Ultra-Wideband Polarization Conversion Meta-Surface and Its Application in RCS Reduction

Jian Yong Yin[1, 2, *], Hou Jun Sun[1], and Lei Zhang[1]

Abstract—In this paper, a novel meta-surface with polarization conversion characteristic in an ultra-wide band is proposed. Based on the principle of the reflected wave cancelation, the proposed meta-surface is distributed as a checkerboard to obtain an ultra-wideband radar cross section (RCS) reduction, resulting from the out-of-phase difference in normal incidence. The relationship between the polarization conversion ratio (PCR) and RCS reduction is investigated and verified by the simulation. Finally, a sample is fabricated and measured in an anechoic chamber. Compared to the metal board with same size, a 5 dB RCS reduction is achieved ranging from 3.7 GHz to 15.9 GHz, which indicates a fractional bandwidth of 124.5%. Moreover, the size of the unit cell is only $0.125\lambda_0 \times 0.125\lambda_0 \times 0.059\lambda_0$, where λ_0 is corresponding to the lowest frequency, namely 3.7 GHz, indicating the merits of miniaturization and low profile. Experiment results are in good agreement with the simulated ones, which demonstrates the validity of the proposed strategy.

1. INTRODUCTION

In recent years, the rapid development of defense electronics has stimulated the research enthusiasm for RCS reduction of military platform extensively, and a number of effective methods have been proposed, in which shaping technology and loading radar absorbing materials (RAMs) are representatives [1, 2]. The former approach can achieve RCS reduction by resorting to deflecting the scattered energy away from the incident wave direction, whereas the latter usually converts the incoming energy into heat instead of backscatter [3, 4]. Because of the ability to manipulate electromagnetic (EM) waves flexibly, varieties of meta-materials or meta-surfaces are proposed and applied to RCS reduction, such as electromagnetic band gap (EBG), artificial magnetic conductor (AMC), polarization conversion meta-surface (PCM), frequency selective surface (FSS), and meta-material absorbers (MA) [5–9]. However, many methods of RCS reduction based on meta-materials or meta-surfaces are restricted in narrow bandwidth.

In order to broaden the RCS reduction, the meta-surface arranged in a checkerboard is proposed. By designing two or more kinds of AMCs and arranging in a periodic or aperiodic checkerboard structure, a $180^\circ \pm 37^\circ$ phase difference can be maintained in a wide bandwidth, which contributes to wideband RCS reduction based on the principle of reflected wave cancelation [10, 11]. Instead of two or more different unit cells, only a uniform unit cell of PCM is designed for wideband RCS reduction, which makes it attract more and more attention. For incident EM wave, a 90° phase shift can be introduced with PCM, while a -90° phase shift can be easily obtained by mirroring the PCM. As a result, by arranging in a checkerboard structure with PCM unit and its mirror, an inherent 180° phase difference of reflected fields can be obtained, and a wideband RCS reduction is achieved [12].

Received 10 September 2019, Accepted 15 December 2019, Scheduled 9 January 2020

* Corresponding author: Lei Zhang (txdy519@163.com).

[1] The School of Information and Electronics, Beijing Institute of Technology, Beijing 100081, China. [2] Space Star Technology Co., Ltd, China Academy of Space Technology, Beijing, China.

In order to broaden the bandwidth of RCS reduction, a lot of wideband PCMs are proposed [13–15]. Reference [16] chooses two pairs of L-shaped patches as PCM. As a result, a wideband RCS reduction is obtained from 10 GHz to 18 GHz. In [17], the PCM and partially reflecting surface (PRS) are employed to achieve wideband RCS reduction and gain enhancement of an antenna simultaneously, and a wideband RCS reduction ranging from 9 GHz to 20 GHz is exhibited. A fishbone-shaped PCM is studied in [18] and applied to achieve a wideband RCS reduction of a slot array antenna. Compared to the reference antenna, the RCS of the antenna with PCM can be reduced more than 5 dB in frequency range from 6 GHz to 18 GHz, indicating a 100% bandwidth. Reference [19] proposes a quasi-L-shaped PCMs and investigates their applications to RCS reduction. The proposed PCMs has a frequency band of 5.98 GHz to 18.84 GHz with the PCR being higher than 50%, which means that a 3 dB RCS reduction can be obtained with a relative bandwidth of 103.6%. A novel wideband low RCS reflector is proposed by employing hexagon polarization rotation surfaces [20]. By optimizing the arrangement, a RCS reduction bandwidth ranging from 8 GHz to 13 GHz is obtained. In [21], a chessboard-type PCM is proposed and applied to achieve a gain enhanced and low RCS circularly polarized patch antenna. Compared to the reference antenna, the gain of proposed antenna is enhanced by 2.5 dB, and a wide RCS reduction bandwidth is obtained from 7.55 GHz to 20.74 GHz.

In this paper, a novel ultra-wideband PCM is presented. By arranging the PCM in a checkerboard, an ultra-wide 5 dB RCS reduction bandwidth ranging from 3.7 GHz to 15.7 GHz can be obtained. Compared with other references in open literature using PCM, the proposed PCM has a more compact structure and lower profile, and can achieve RCS reduction in a wider frequency range.

2. UNIT CELL DESIGN OF ULTRA-WIDEBAND POLARIZATION CONVERSION META-SURFACE

The proposed unit cell of PCM is depicted in Fig. 1, and it consists of five square patches on a Taconic-TLY dielectric substrate backed by a PEC sheet, in which the relative permittivity and loss tangent of substrate are 2.2 and 0.0009, respectively. Based on multiple resonances, five square patches with different sizes are employed and interconnected in a line along 45° diagonal direction so as to broaden the PCR bandwidth. By optimizing the structural parameters carefully with High Frequency Structure Simulator (HFSS), an ultra-wide polarization conversion bandwidth is obtained, and the optimized parameters are as follows: $p = 10$ mm, $a = 3.6$ mm, $b = 1.8$ mm, $c = 0.8$ mm, $t = 4.72$ mm.

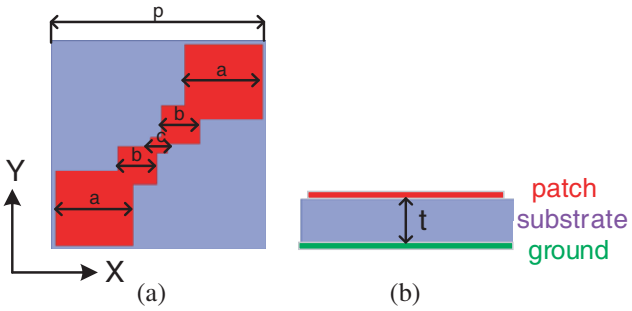

Figure 1. Topological structure of the proposed unit cell. (a) Top view. (b) Side view

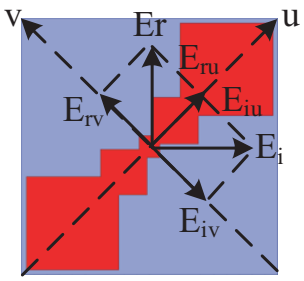

Figure 2. The procedure of polarization conversion.

The polarization conversion principle can be explained as follows. Suppose that a plane EM wave with the polarization of $\overrightarrow{E_1}$ is impinging on the meta-surface in the normal incidence. A coordinate system can be set up along two orthogonal directions $\vec{u}$ and $\vec{v}$, then the incident wave can be expressed as follows:

$$\overrightarrow{E_l} = \overrightarrow{E_{lu}} + \overrightarrow{E_{lv}} = \vec{u}E_{iu}e^{j\varnothing} + \vec{v}E_{iv}e^{j\varnothing} \tag{1}$$

When the meta-surface has different reflection properties for the u-incident wave and v-incident wave, denoted as $r_u e^{j\varnothing_u}$ and $r_v e^{j\varnothing_v}$ respectively, the reflected wave can be shown as follows:

$$\overrightarrow{E_r} = \overrightarrow{E_{ru}} + \overrightarrow{E_{rv}} = \vec{u}r_u e^{j\varnothing_u}E_{iu}e^{j\varnothing} + \vec{v}r_v e^{j\varnothing_v}E_{iv}e^{j\varnothing} \tag{2}$$

If the following conditions can be met,

$$\begin{cases} r_u = r_v \\ \Delta\varnothing = |\varnothing_u - \varnothing_v| = 180^\circ \end{cases} \tag{3}$$

then the electric field is rotated into its orthogonal component, and the procedure can be depicted as Fig. 2.

The reflection coefficients of u-incident wave and v-incident wave and the phase difference between them are shown in Fig. 3. It can be seen that at 4.2 GHz, 8.8 GHz, and 15 GHz, the magnitude and phase difference between u-incident wave and v-incident wave fulfill Equation (3), which indicates that the incident polarized wave is fully converted into the orthogonal component, whereas in the rest of frequency range, only part of the incident polarized component is converted. In order to demonstrate the polarization conversion ratio (PCR) of the proposed meta-surface, the relative parameters are defined as follows: $r_{xy} = |E_x^r/E_y^i|$ and $r_{yy} = |E_y^r/E_y^i|$ are the reflection ratio of y-to-x and y-to-y polarization conversion, in which E^r and E^i represent the reflected electric field and incident electric field, while E_x and E_y represent the x-polarized and y-polarized electric fields, respectively. As a result, the PCR can be expressed as $\text{PCR} = |r_{xy}|^2/(|r_{xy}|^2 + |r_{yy}|^2)$.

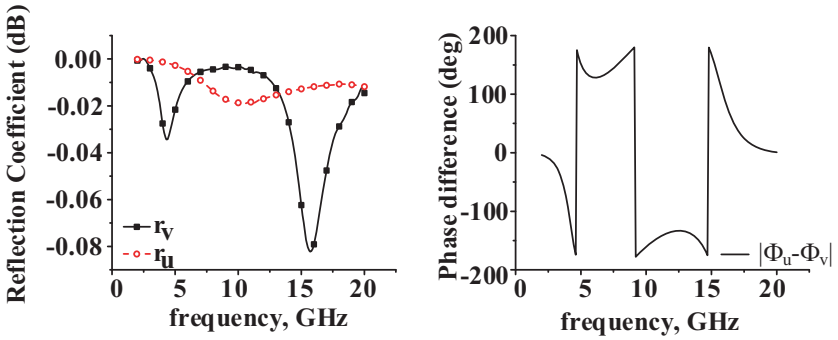

Figure 3. Reflection coefficient and phase difference between the u-incident wave and v-incident wave. (a) Reflection coefficient. (b) Phase difference.

The simulated reflection ratio of unit cell and calculated PCR are listed in Fig. 4 with periodic boundary condition for the incident y-polarized plane wave in normal direction. It is clear that in the frequency range from 3.6 GHz to 15.9 GHz, the PCR of the proposed PCM is higher than 50%, which means that at least half of the incident y-polarized wave is converted into the x-polarized component. In particular, at 4.2 GHz, 8.8 GHz, and 15 GHz, the PCR is nearly 100%, which agrees with above statements.

In order to investigate how parameters affect the PCR of the proposed PCM, a series of parameter analysis is exhibited in Fig. 5 in the case that only one parameter changes, and the others are fixed. It

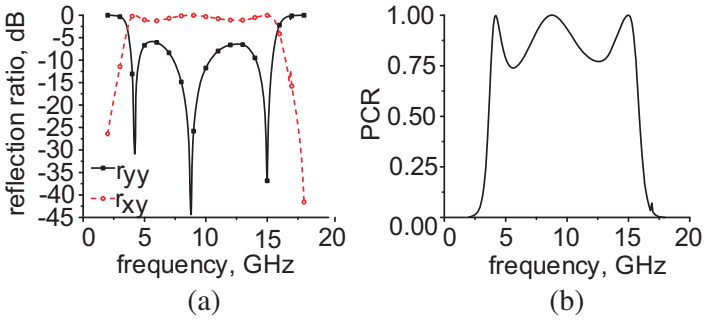

Figure 4. Reflection ratio and calculated PCR of unit cell. (a) Reflection ratio. (b) PCR.

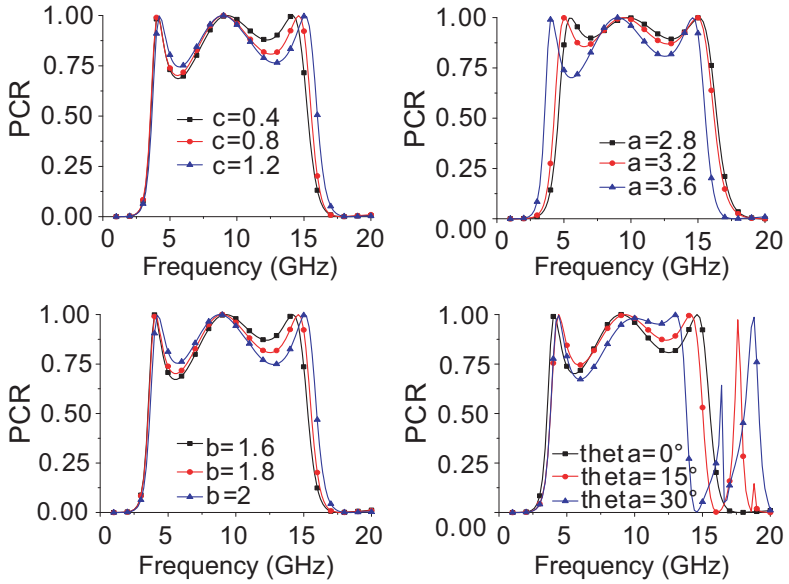

Figure 5. The effect on PCR with different parameters.

can be seen that parameters c and b mainly influence the resonance in higher frequency band. Because of their compact size, the changes in parameter c and b make a little contribution to broadening the bandwidth of PCR. The resonance in the lower frequency is decided by parameter a. As parameter a is increased, the frequency band of PCR moves to a lower frequency, while the PCR among three resonant frequency points gets worse. Making a compromise of the PCR, bandwidth, and its compact size, parameter a is selected as 3.6 mm. The PCR curves versus frequency with different incident angles are also shown in Fig. 5. When the incident angle increases from 0° to 30°, the frequency response below 15 GHz is kept stable, while the third resonant frequency point moves to the lower frequency, and the PCR bandwidth decreases.

3. THE CHECKERBOARD AND ITS ULTRA-WIDEBAND RCS REDUCTION

By taking advantage of the ultra-wideband polarization conversion characteristic, the proposed metasurface can be assembled in a checkerboard, as shown in Fig. 6. For the x-polarized incident wave, the reflected wave is y-polarized and $-y$-polarized converted by the proposed checkerboard, and an inherent 180° phase difference between reflected fields can be obtained, resulting in an ultra-wideband RCS reduction, compared to the same-size metal board as the reference.

Compared to the same-size metal board, the relationship between the RCS reduction and PCR is

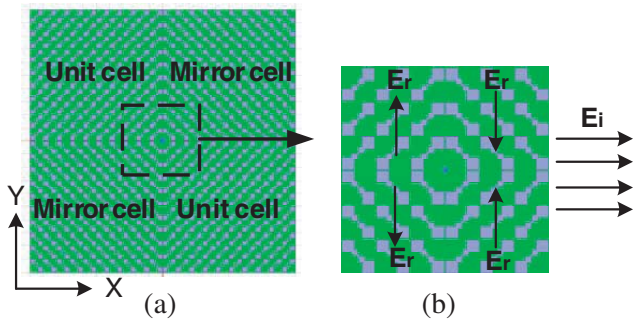

Figure 6. Configuration of the checkerboard.

approximately listed in Eq. (4)

$$\text{RCS Reduction} = -10\log_{10}(1 - \text{PCR}) \tag{4}$$

in which the employed unit is decibel (dB). The simulated RCS reduction and calculated RCS reduction based on the PCM are compared in Fig. 7, in which it can be seen that the simulated result agrees well with the calculated one, and the distinguish between them is rooted in the simulation conditions. The simulated result is derived from the full wave EM simulation with 20×20 unit cells by high frequency structure simulation (HFSS), while the calculated result is derived from the simulation in periodic boundary condition, indicating infinite unit cells.

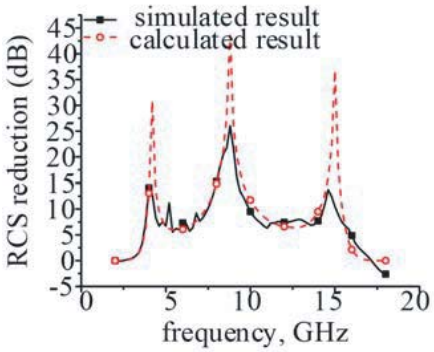

Figure 7. The comparison of the simulated and calculated RCS reduction.

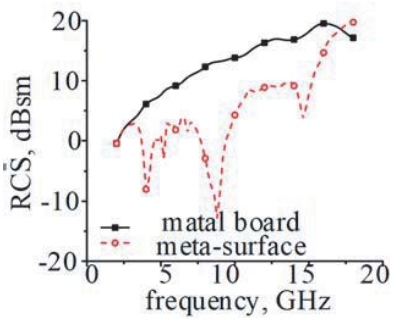

Figure 8. Comparison of monostatic RCS for normal incidence.

Figure 8 shows the monostatic RCS of the proposed checkerboard meta-surface and the metal board with EM wave impinging from the normal direction. It can be seen that compared to the metal board, the checkerboard meta-surface has a lower RCS value in an ultra-wide frequency range from 2.5 GHz to 17.2 GHz, in which the maximum of RCS reduction is as much as 26 dB at 8.8 GHz.

In order to demonstrate the scattering cancellation, Fig. 9 shows the 3-D bistatic RCS of the proposed checkerboard and the same-size PEC plane with EM wave impinging from the normal direction at 8.8 GHz. It can be seen that there is a main lobe in the backward of the incident direction for the scattered energy of PEC. Instead, four sidelobes in the other direction for the scattered energy of the proposed checkerboard arise, while the main lobe is suppressed. It means that the incident energy is converted and deflected into other direction instead of backward, which leads to a monostatic RCS reduction. Fig. 10 shows the bistatic RCS comparison between the proposed checkerboard and the referred PEC with the EM wave impinging in oblique incident direction at 8.8 GHz for dual polarizations.

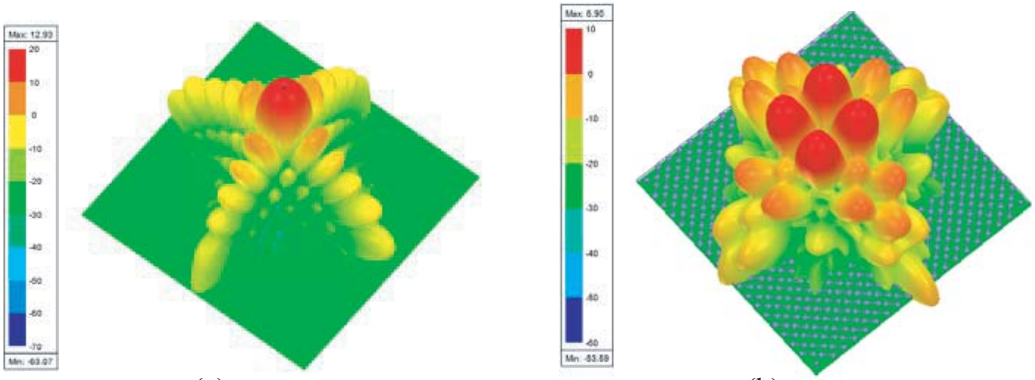

Figure 9. 3-D bistatic RCS at 8.8 GHz for normal incidence. (a) PEC. (b) Proposed checkerboard.

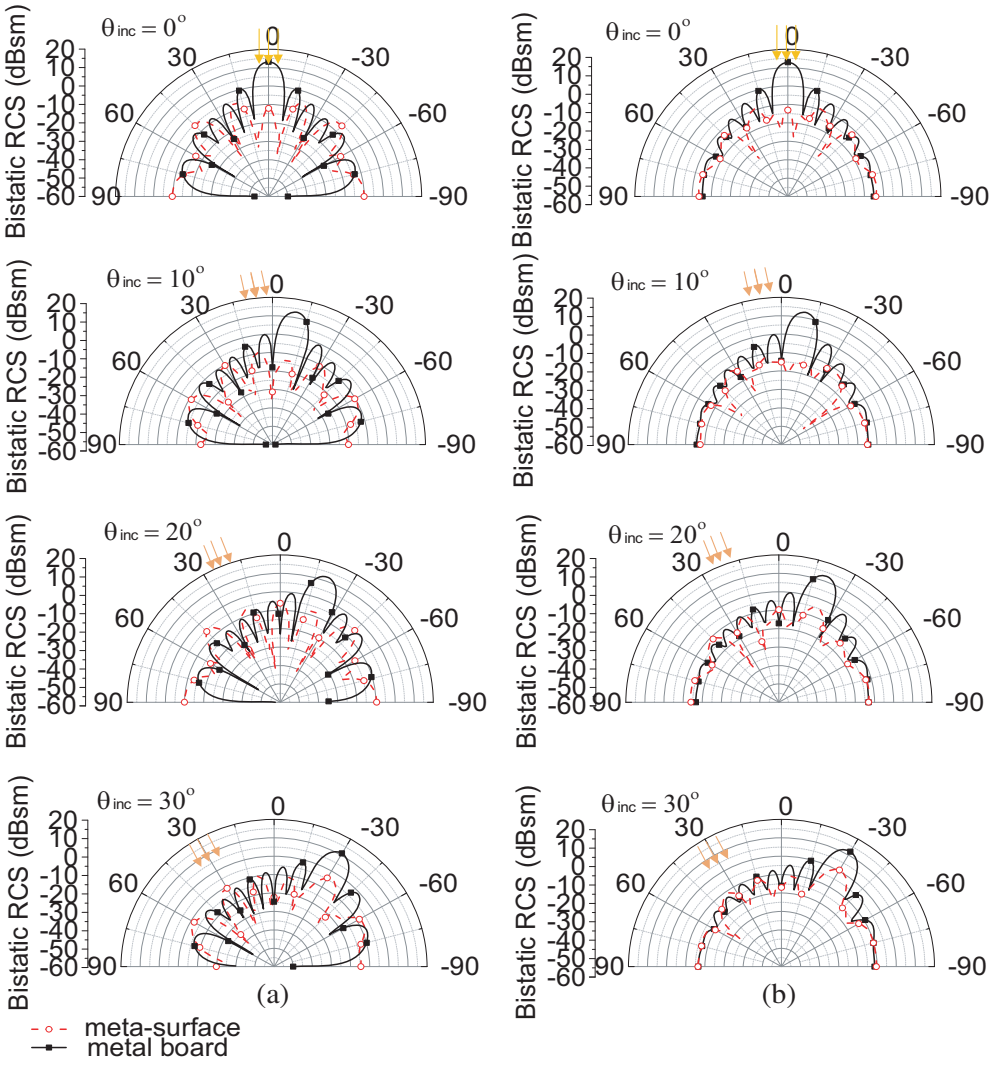

Figure 10. Bistatic RCS at 8.8 GHz for different incident angle. (a) ϕ-polarization. (b) θ-polarization.

It can be observed that as the incident angle increases from 0° to 30°, an RCS reduction more than 10 dB can be obtained for dual polarizations, respectively.

4. FABRICATION AND MEASUREMENT

In order to verify the validity of the proposed strategy, a sample with the dimension of $200 \times 200\,\text{mm}^2$ is fabricated, and its fabricated prototype is exhibited in Fig. 11. The RCS of the fabricated prototype and the metal broad with the same size are measured in an anechoic chamber. The curves of RCS reduction versus frequency of measured results are shown in Fig. 12, and a more than 5 dB bandwidth can be obtained from 3.7 GHz to 15.7 GHz, indicating a fractional bandwidth of 124.5%, which is in accordance with the PCR higher than 68.4% based on Equation (4). The average RCS reduction in the whole band is 14 dB. It can be seen that the measured result agrees well with the simulated one, indicating the validity of the proposed strategy. Meanwhile, discrepancies can be observed between the simulated and measured results, which may come from alignment in the measurement setup, imperfection of the environment in the chamber, deviation of permittivity of the substrate, and fabrication tolerance.

In Table 1, a comparison of electric size of PCM and RCS reduction bandwidth between the proposed checkerboard meta-surface and the other reported wideband checkerboard design by employing

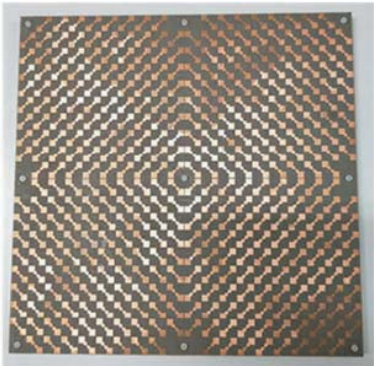

Figure 11. The fabricated prototype of the proposed checkerboard meta-surface.

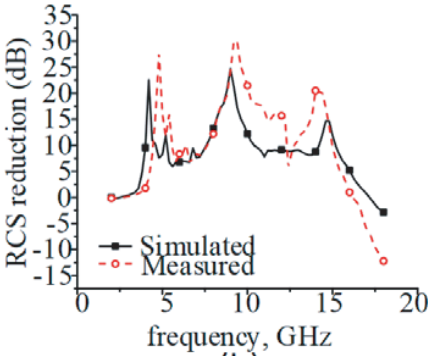

Figure 12. Comparison of RCS reduction between simulated and measured results.

Table 1. Comparison with the other PCM in the open literature.

Ref.	Size (λ^3)	Average RCS reduction	RCS reduction bandwidth
[12]	$0.23 \times 0.23 \times 0.073$	> 4.8 dB	10.5 GHz $\sim$ 35.1 GHz (107.9%)
[13]	$0.184 \times 0.184 \times 0.089$	12.97 dB	4 GHz $\sim$ 15 GHz (115.8%)
[14]	$0.21 \times 0.21 \times 0.077$	> 5 dB	6.3 $\sim$ 20.7 GHz (106.7%)
[15]	$0.138 \times 0.138 \times 0.069$	> 8 dB	6.9 GHz to 14.9 GHz (73.3%)
[17]	$0.195 \times 0.195 \times 0.078$	12.36 dB	9 GHz $\sim$ 20 GHz (75.9%)
[18]	$0.12 \times 0.12 \times 0.06$	> 5 dB	6 GHz $\sim$ 18 GHz (100%)
[19]	$0.24 \times 0.24 \times 0.06$	> 3 dB	5.98 GHz $\sim$ 18.84 GHz (103.6)
[21]	$2.18 \times 2.18 \times 0.082$	11 dB	7.55 GHz $\sim$ 20.75 GHz (93.25%)
This paper	$0.12 \times 0.12 \times 0.058$	14 dB	3.7 GHz $\sim$ 15.9 GHz (124.5%)

PCM is presented. It is clear that the proposed checkerboard meta-surface based on the novel PCM in this paper has an obvious advantage on RCS reduction bandwidth, while it can also keep a compact structure and low profile.

5. CONCLUSION

In this paper, a simple PCM with ultra-wide polarization conversion characteristic is proposed and employed to form a checkerboard surface to achieve ultra-wideband RCS reduction. Simulated and measured results show that compared to the same-size metal board, the RCS of the designed checkerboard surface can be reduced more than 5 dB in the range from 3.7 GHz to 15.9 GHz, exhibiting an ultra-wideband characteristic with a fractional bandwidth of 124.5%. At meantime, the proposed PCM also has the merits of miniaturization and low profile. Experiment results demonstrate the validity of the proposed method.

REFERENCES

1. Knott, E. F., J. F. Shaeffer, and M. T. Tuley, *Radar Cross Section*, SciTech Publishing, Raleigh, 2004.
2. Han, Z. J., W. Song, and X. Q. Sheng, "Gain enhancement and RCS reduction for patch antenna by using polarization dependent EBG surface," *IEEE Antennas Wireless Propag. Lett.*, Vol. 16, 1631–1634, 2017.

3. Li, W. Q., X. Y. Cao, J. Gao, et al., "A novel low RCS microstrip antenna," *3th Asia-Pacific Conference on Antennas and Propagation*, 495–498, Harbin, China, August 2014.
4. Dikmen, C. M., S. Cimen, and G. Cakir, "Planar octagonal-shaped UWB antenna with reduced radar cross section," *IEEE Trans. Antennas Propag.*, Vol. 62, No. 6, 2946–2953, 2014.
5. Su, J. X., C. Y. Kong, Z. R. Li, et al., "Wideband diffuse scattering and RCS reduction of microstrip antenna array based on coding metasurface," *Electron. Lett.*, Vol. 53, No. 16, 1088–1090, 2017
6. Zhang, J. J., J. H. Wang, M. E. Chen, et al., "RCS reduction of patch array antenna by electromagnetic band-gap structure," *IEEE Antennas Wireless Propag. Lett.*, Vol. 11, 1048–1051, 2012.
7. Shi, Y., Z. K. Meng, W. Y. Wei, et al., " Characteristic mode cancellation method and its application for antenna RCS reduction," *IEEE Antennas Wireless Propag. Lett.*, Vol. 18, No. 9, 1784–1788, 2019.
8. Shi, Y., X. F. Zhang, Z. K. Meng, et al., " Design of low RCS antenna using antenna array," *IEEE Trans. Antennas Propag.*, Vol. 67, No. 10, 6484–6493, 2019.
9. Kundu, D., S. Baghel, A. Mohan, et al., "Design and analysis of printed lossy capacitive surface-based ultrawideband low profile absorber," *IEEE Trans. Antennas Propag.*, Vol. 67, No. 5, 3533–3538, 2019.
10. Zaki, B., Z. H. Firouzeh, Z. N. Abolgasem, et al., "Wideband RCS reduction using three different implementations of AMC structures," *IET Microw. Antennas Propag.*, Vol. 13, No. 5, 533–540, 2019.
11. Song, X. Y., Z. H. Yan, and T. L. Zhang, "Broadband AMC surface for radar cross section reduction," *ICMMT*, 2018.
12. Hong, T., S. Wang, Z. Y. Liu, et al., "RCS reduction and gain enhancement for the circularly polarized array by polarization conversion metasurface coating," *IEEE Antennas Wireless Propag. Lett.*, Vol. 18, No. 1, 167–171, 2019.
13. Sun, S. Y., W. Jiang, X. Q. Li, et al., "Ultrawideband high-efficiency 2.5-dimensional polarization conversion metasurface and its application in RCS reduction of antenna," *IEEE Antennas Wireless Propag. Lett.*, Vol. 18, No. 5, 881–885, 2019.
14. Chen, W. K., J. F. Shi, Z. Y. Niu, et al., "Broadband polarization conversion metasurface for radar cross section reduction," *ICMMT*, 2018.
15. Wang, J. X., S. Shang, D. W. Song, et al., "RCS reduction of a microstrip patch based on broadband PRRS," *ISAPE*, 2018.
16. Zou, S. X., J. L. Wei, and X. Man, "Wideband RCS reduction of patch antenna using PRRS," *Electron. Lett.*, Vol. 53, No. 8, 522–524, 2017.
17. Long, M., W. Jiang, and S. X. Gong, "Wideband RCS reduction using polarisation conversion metasurface and partially reflecting surface," *IEEE Antennas Wireless Propag. Lett.*, Vol. 16, 2534–2537, 2017.
18. Liu, Y., K. Li, Y. T. Jia, Y. W. Hao, S. X. Gong, and Y. J. Guo, "Wideband RCS reduction of a slot array antenna using polarisation conversion metasurfaces," *IEEE Trans. Antennas Propag.*, Vol. 64, No. 1, 326–331, 2016.
19. Jia, Y. T., Y. Liu, Y. J. Guo, et al., "Broadband polarisation rotation reflective surfaces and their applications to RCS reduction," *IEEE Trans. Antennas Propag.*, Vol. 64, No. 1, 179–188, 2016.
20. Deng, Z. H., F. W. Wang, Y. H. Ren, et al., "A novel wideband low-RCS reflector by hexagon polarization rotation surfaces," *IEE Access*, Vol. 7, 131527–131533, 2019.
21. Liu, Z. S., Y. Liu, and S. X. Gong, "Gain enhanced circularly polarized antenna with RCS reduction based on metasurface," *IEEE Access*, Vol. 6, 46856–46862, 2018.